A systematic approach for conducting and interpreting hydraulic conductivity tests on granular soils under non-isothermal conditions

Marina S. Bortolotto[1#], *David M. G.* Taborda[1], and *Catherine* O'Sullivan[1]

[1]*Imperial College London, Department of Civil and Environmental Engineering, London, UK*
[#]*Corresponding author: marina.bortolotto@imperial.ac.uk*

ABSTRACT

Although non-isothermal tests are important for many applications in geotechnical engineering, there is no standard for conducting such tests and interpreting the resulting data. This paper describes the development of a temperature-controlled triaxial apparatus, focussing on its thermal performance, and discusses relevant protocols to perform and interpret hydraulic conductivity tests on granular materials at different temperatures. With the aid of thermal cameras, hot spots on the surface of the equipment and instruments were identified. Subsequent modifications to minimise and mitigate heat reaching volume gauges and pore water pressure transducers were introduced. After modifications to reduce the system's intrinsic head losses, the thermal expansion of the system proved to be significant and needed to be accounted for avoiding overestimation of thermally-induced mechanical strains. The addition of a new probe at the centre of the specimen allowed the characterisation of the temperature field within the system and specimen, as well as assisting with the identification of thermal equilibrium. Significant drops in temperature were flagged by this probe, though these proved to be unimportant in terms of hydraulic conductivity. The use of the average temperature for each pressure step is advised when a specimen probe is available. Alternatively, the use of target temperatures can be chosen, leading to minor underestimations of the intrinsic permeability.

Keywords: non-isothermal test; hydraulic conductivity; granular material; thermal camera.

1. Introduction

The use of temperature-controlled apparatuses dates back to the 1950's with the adaption of an isothermal oedometer to test clays (Finn 1952). Campanella and Mitchell (1968) were the first to develop a temperature-controlled triaxial apparatus and ever since many different apparatuses capable of subjecting soil samples to complex stress paths under non-isothermal conditions have been adapted, such as the hollow cylinder (e.g. Liu et al. 2018) and true triaxial (e.g. Russel Coccia and McCartney 2012). Despite this continuous development of equipment, there is still no standard protocol for performing non-isothermal testing of soils.

The lack of standards for non-isothermal tests that delimit acceptable variations and determine rigorous procedures and calibrations that should produce high-quality and repeatable results to be then interpreted in a consistent manner can lead to unacceptable variations and even inconsistent results. This is especially relevant when the linear coefficient of thermal expansion of minerals is of the order of magnitude of 10^{-6} m/(m·K) and expected volumetric strains are as small as 0.01% (Pan, Coulibaly, and Rotta Loria 2021). As a consequence, the best approach at the moment might be to use isothermal standards as general guidelines and to critically expand the testing procedures whenever necessary. This requires attention to characterize and improve accuracy, minimize errors (Pan, Coulibaly, and Rotta Loria 2021), calibrate and understand the limitations of equipment and testing procedures (Cekerevac, Laloui, and Vulliet 2005; Jaradat and Abdelaziz 2020; Abdelaziz and Morteza Zeinali 2022).

Usually, non-isothermal equipment is adapted from an isothermal equivalent, employing instruments that are often highly affected by temperature; this can lead to excessively large errors and, hence, unreliable results. While there is not yet great development on instruments that can endure temperature changes without having their performance affected, special attention needs to be paid to the measurement of the temperature field to which such instruments are subjected, the corresponding impact of such temperatures and, if necessary, what actions are required to quantify and mitigate it (either by adapting the calibration procedure or by modifying the equipment design). The focus of the present work is to highlight possible errors due to heat reaching instrumentation and provide alternatives of how to measure, minimize or mitigate, and possibly account for such thermal effects on the results obtained when using the Imperial College MKII permeameter.

2. Imperial College MKII permeameter

The Imperial College MKII permeameter is a bespoke temperature-controlled triaxial apparatus capable of performing hydraulic conductivity tests and represents the latest design of MK cells (Bortolotto, Taborda, and

O'Sullivan 2022). Martinez-Calonge (2017) introduced the first design of temperature-controlled triaxial, designated as MKI. The most significant difference between the two designs is how heat is applied, with the MKII cell being essentially a conventional high-pressure isothermal triaxial cell submerged into a (non-pressurised) thermal bath – similar to the temperature-controlled oedometer developed by Kirkham, Tsiampousi, and Potts (2018).

A circulatory pump connected to the bottom and top of the thermal bath contributes to achieving a more homogeneous heat distribution along the surface of the triaxial cell. An extra temperature probe was added to the pedestal of the equipment (positioned right at the centre of the specimen) to improve the characterisation of the temperature field in the equipment and specimen (this is described in detail in Section 2.2). Therefore, the system currently has four temperature probes that are positioned: i) within the PVC water jacket (i.e. non-pressurised ring); ii) inside the triaxial cell (inner cell); iii) embedded into the pedestal; and iv) at the centre of the specimen. The system currently accommodates specimens that are 100 mm high and 50 mm in diameter. This MKII permeameter was first presented in detail by Bortolotto, Taborda, and O'Sullivan (2022), where a thorough description of the equipment and individual parts is provided. Further development of this equipment, particularly in terms of the thermal response and behaviour of the system, is the focus of the present work.

The system has three independent pressure systems that control the cell pressure (up to 5 MPa of isotropic stress), and the two components of the back pressure that are connected to top and bottom of the specimen. Each independent system has its own air-water interface and pore water pressure (pwp) transducer. Back pressure systems are controlled by 100 cm^3 Imperial College volume gauges (Fig 1, "TVG" and "BVG") that also measure flow rate. Pwp transducers are positioned between the bottom and top of the specimen and their respective volume gauges. These transducers are connected to mounting blocks that are rigid enough to not insert extra compliance to the system. Section 2.1 focusses on describing several components of this equipment, which are illustrated in Fig. 1: the valve ("A") connecting the transducer mounting block ("B") to the drainage line going to the top of the specimen, volume gauges connected to the top of the specimen ("TVG") and to the base of the specimen ("BVG"), drainage lines between mounting blocks and volume gauges ("BB" and "TB" for the base and top of the specimen, respectively), the top pwp transducer ("TPT") and respective spacer ("TS").

It is important to introduce the nomenclature adopted in this paper. The drainage system is understood to be any and all elements of the back pressure system, i.e. between the top and bottom volume gauge: mounting blocks, valves, pwp transducers, the tubes themselves, porous stones and drainage lines inside the pedestal and top cap. Drainage lines usually refer to the tubes themselves. When discussing the portion of the drainage system that might be affected by temperature (Sections 2.1 to 2.3), the porous stones, drainage lines within pedestal and top cap, tubes inside the system and part of these tubes after exiting the system are included.

Calibrations to isolate the response of the system are extremely important. Therefore, procedures to characterize the system's intrinsic head losses (Section 3.1) and the system's thermal expansion/contraction (Section 2.3) are described. Instead of a soil specimen, calibrations were performed using a hollow PVC cylinder ($Ø_{int}$=41.5 mm) filled with freshly de-aired water placed between the porous stones. The thermal response of this cylinder was calculated and then subtracted from measured values during calibration.

The importance of post-processing data in terms of intrinsic permeability as an attempt to remove effects of temperature on water density and dynamic viscosity is presented in Section 3.2.

A loose specimen of Hostun sand is used throughout this paper to illustrate temperature effects on a real soil specimen. Hostun sand is a fine-uniform-siliceous sand physically characterised by Azeiteiro et al. (2017). The specimen considered here is fully saturated, with a relative density of 25.9% (e=0.905) after being isotropically consolidated under 100 kPa at room temperature – before any non-isothermal test.

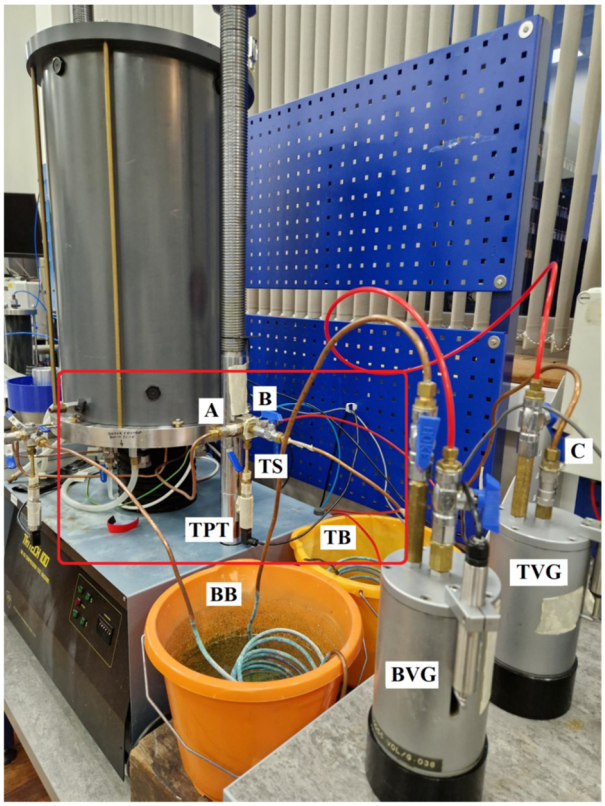

Figure 1. Side view of temperature-controlled triaxial apparatus (Imperial College MKII permeameter) with details indicating measuring areas used on thermal images: A) valve connecting top of the specimen to top mounting block; B) top mounting block; C) entrance of top volume gauge. Top spacer (TS) separating mounting block and respective pwp transducer (TPT). Heat exchangers (TB, BB) submerged in thermal baths and connecting the mounting blocks to respective volume gauges (TVG and BVG).

2.1. Thermal camera

Two thermal cameras were used to identify hot spots on the surface of the system and its elements, such as the drainage system. Both thermal cameras used in the present work are Optris Xi 400 capable of measuring temperatures between -20°C and 100°C, and accuracy of ±2%. The manufacturer's software not only records (static) images in ".tiff" format that allows analysis of the temperature of every single pixel, but also records videos that allow temperature time-histories to be established for each point. Moreover, multiple measurement areas can be set and exported as ".csv" for determining the temperature variation of each individual area, which might flag the need to investigate specific spots with a temperature sensor.

Due to the transient nature of hydraulic conductivity tests and heat transfer that occurs through key elements of the system, the use of thermal cameras provides incredibly helpful insights into the thermal performance of the equipment before and after interventions.

Measuring areas of one single pixel are analysed. The points A, B, C, TS and TPT indicated in Fig. 1 are monitoring points and will be used in the following subsections for further analysis with the aid of thermal cameras. Due to the variety of materials in the equipment and, correspondingly, different emissivity and reflection values, key elements are covered with masking tape to improve the accuracy of measurements.

2.1.1. Heat exchangers

Drainage lines entering both volume gauges were monitored to infer the temperature of the fluid reaching the volume gauges. Temperatures of up to 37.9°C were measured at these key elements while performing hydraulic conductivity tests at 60°C under a theoretical pressure differential of 12 kPa.

The imposed pressure differential affects measured temperatures since different velocities are expected and, therefore, warm water has more or less time to lose heat to the environment as it travels from the specimen to the instrumentation (Fig. 2). Moreover, as warm water travels, heat is lost to different parts of the equipment, and the temperature of these parts builds up over time (Fig. 2). This means that the temperature of an instrument changes over time even for conditions of constant (target) temperature and pressure differential. Because of the transient nature of heat transfer, calibrating volume gauges at different temperatures is impractical. Consequently, the equipment was modified to minimise the heat reaching volume gauges and, hence, enabling their use under isothermal conditions independently of the target temperature and pressure differential.

Initially, both volume gauges were connected to their respective mounting blocks through short (about 40 cm) nylon tubes. The abovementioned temperature of 37.9°C was measured at the entrance of the bottom volume gauge (point "C") while the "inlet" temperature immediately before its mounting block (point "A") was 43.2°C. The first intervention consisted of switching these 40cm-longer tubes by much longer (approximately 3 m) coiled-shaped nylon tubes that were submerged in a thermal bath at room temperature. The coiled tubes work as heat exchangers, resulting in a reduction of more than 10°C at point "C" for the same "inlet" temperature of 43.2°C. However, the temperature at point "C" (26.2°C) was still higher than the room temperature (21°C ±1°C). Therefore, a second modification was introduced, replacing the material used for the heat exchangers by another with higher thermal conductivity, thus facilitating the exchange of heat between the water inside the tubes and the thermal bath. Consequently, 3m-long coiled-shaped copper tubes are used as heat exchangers and also submerged into the thermal baths. This resulted in the temperatures at point "C" being virtually equal to room temperature even when the "inlet" temperature was still 43.2°C. Fig. 2 presents the surface temperature of the described monitoring points captured by the thermal cameras and compare values before and after the introduced modifications.

2.1.2. Pore-water pressure transducer spacer

Chen, Zdravkovic, and Carraro (2019) investigated temperature effects on pwp transducers positioned outside the triaxial cell and on a mid-height pwp probe positioned within the cell. While the mid-height pwp probe is directly subjected to the temperature of the equipment (20°C to 60°C), it seems that the external pwp transducer is not significantly affected by the equipment's temperature since a single calibration factor (independent of temperature) is proposed. The mid-height pwp probe, however, requires different calibration factors that are temperature dependent. Their observations are valid for the reported conditions, which are slightly distinct from those the MKII pwp transducers are subjected to.

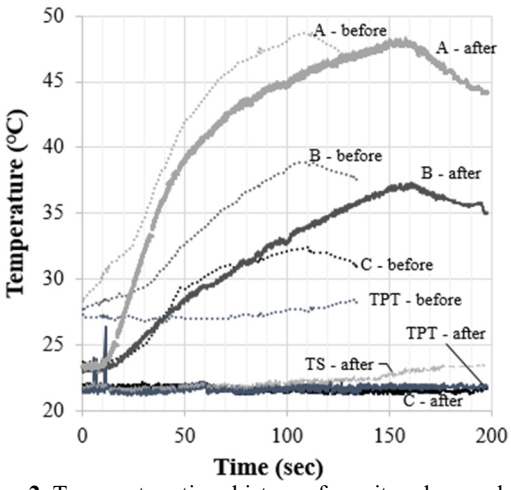

Figure 2. Temperature time-history of monitored areas during hydraulic conductivity tests at 60°C using thermal cameras. Curves correspond to points presented in Fig.1 for the top portion of drainage line: "A" valve coming from the specimen; "B" mounting block; "C" entrance of volume gauge; "TPT" pwp transducer, and "TS" spacer between mounting block and pwp transducer. Dotted lines correspond to the initial configuration of the system ("before"), while solid lines correspond to the current configuration ("after" interventions).

Similar to volume gauges, the two pwp transducers connected to the drainage lines were also subjected to transient temperatures during non-isothermal hydraulic conductivity tests. For instance, a gradual increase up to 8°C on the top pwp transducer's surface could be

observed. Variations in the temperature imposed on the pwp transducers can affect pwp measurements, as reported by Chen, Zdravkovic, and Carraro (2019), and possibly return inaccurate values of pore pressure. These are rather important in the context of hydraulic conductivity testing since even small pore water pressure differences can lead to the amplification of errors and uncertainty, particularly when applying the smallest pressure differential of 4 kPa.

Once again, it is desirable to avoid warm water heating the pwp transducers, due to the difficulties associated with calibrating pwp transducers under conditions similar to those observed during hydraulic conductivity tests.

The alternative was to increase the physical distance between pwp transducers and the path followed by the warm water. Spacers (48-mm long) made of brass were fitted between the bottom of mounting blocks and the top of the pwp transducers. After such intervention, the maximum temperature observed on the transducers' surface was of about 22°C. An example of this can be observed in Fig. 2, where the top pwp transducer ("TPT – after") has a roughly constant temperature throughout the test, while the respective spacer ("TS – after") has a relatively small but consistent increase with time.

2.2. Specimen temperature probe

A fourth temperature probe was added at the centre of the specimen (Fig. 3). The thermocouple is positioned at the extremity of a hollow brass rod (external diameter ~6.6 mm), which is approximately 50 mm long in order to be positioned at half of the height of the specimen. This was the smallest diameter possible given the size of the thermocouple and, since granular specimens are commonly prepared using a funnel or air/water deposition, the influence of the probe was judged to be negligible. Brass was chosen not only to provide protection against pressurised water, but also due to its high thermal conductivity.

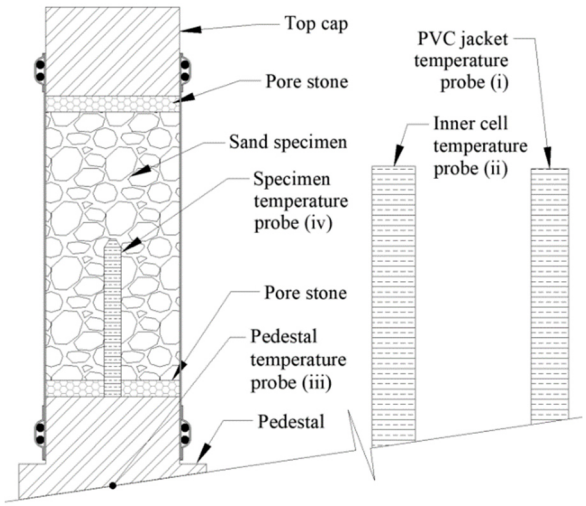

Figure 3. Schematical cross-section of specimen with its temperature probe (iv) positioned right at its center. PVC jacket and inner cell temperature probes are inserted in the represented brass rods (i and ii), the embedded pedestal temperature probe (iii) is also indicated.

The addition of the specimen thermal probe was driven by three main reasons: i) to establish the temperature field within the specimen and equipment; ii) to determine the time required for the entire system to reach thermal equilibrium; and iii) to investigate abnormal drifts observed in the volume gauge several hours after the system had already reached the target temperature.

Heating rate curves (Fig. 4 (a)) reach a maximum value usually between 6.5 and 12.0°C/h, depending on the current temperature (i.e. higher heating rates are observed for stages where the cell temperature is higher). Both the inner cell and the specimen heating rate curves have comparable shapes (for the same stage) with a clear delay being observed for the specimen probe, which is consistent for all investigated temperatures. This is expected because the specimen probe is positioned in the most central region of the equipment and heat is gradually transmitted radially from outer regions to more central ones.

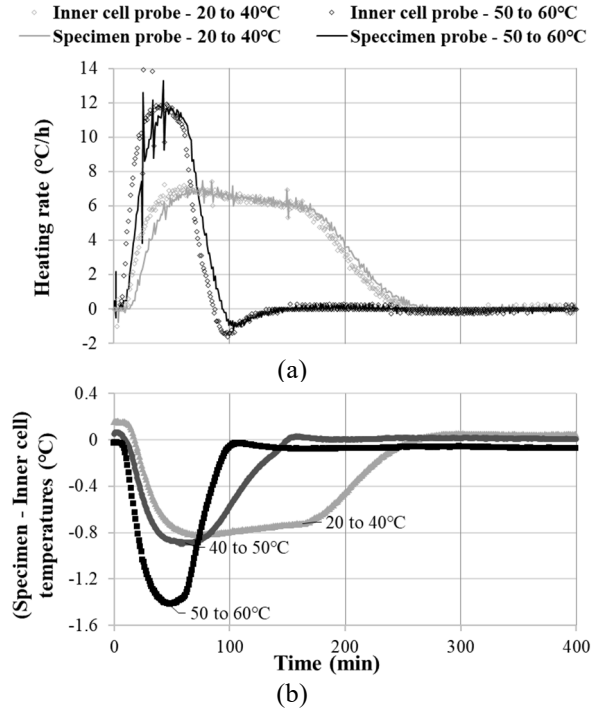

Figure 4. Tests on loose specimen of Hostun sand. (a) Heating rate curves of two different heating stages (20 to 40°C and 50 to 60°C) for two temperature probes: inner cell (circles) and specimen (solid line) over time. (b) Temperature difference between probes (specimen and inner cell) over time for different heating stages.

Both ranges of heating rates are higher than the rate adopted by Liu et al. (2018) for calibrations (5°C/h) using a metallic dummy sample 200 mm high and 100 mm in diameter. Since their specimens are bigger, it might be beneficial to impose this slower rate that guarantees a smaller thermal gradient across the specimen. For 50×100-mm-MKII specimens, however, the maximum temperature difference observed between the inner cell and specimen probes was limited to 1.4°C (Fig. 4 (b)). This value is judged to not be excessive since it rapidly decreases, and it does not necessarily represent the gradient across the specimen because the inner cell probe is positioned 78 mm away from the surface of the

specimen. Given that the radius of the specimen is only 25 mm and that the thermal conductivity of water (0.60 W/m/K) is much smaller than that of saturated quartz sand (approximately 2.54 W/m/K (Mitchell and Soga 2005; Chen 2008)), it is likely that the greatest temperature drop (and hence largest thermal gradient) occurs within the water. This assumes that heat is being transferred solely through diffusion, which is unlikely to be the case in the water where natural convection is expected to be important.

Thermal equilibrium is evaluated using two criteria which relate to: (i) the temperature difference between the inner cell and specimen probes (e.g. Fig. 4 (b)); and (ii) change in volume over time. The first requirement is considered to be achieved when the temperature difference between the specimen and inner cell probes is about the same as during tests at room temperature (±0.4°C). Once the first requirement is fulfilled, which means there is virtually no heat transfer taking place, stable volumetric variations (measured by the volume gauge) over time should be observed without any visible drift. However, as reported before (Bortolotto, Taborda, and O'Sullivan 2022), drifts were observed in the volume gauge after requirement (i) was achieved and this was possibly attributed to non-recoverable deformations experienced by the nylon drainage lines. This abnormal drift could also be attributed to creep of the soil specimen; however, this was disproved by drift being also observed during calibration tests (i.e. without soil specimen). These findings agreed with those reported by Martinez-Calonge (2017).

Given the above, nylon drainage lines were switched to a combination of copper, stainless steel, and brass lines with only two small nylon segments remaining in order to provide flexibility to the top cap and avoid imposing any strains to the specimen during top cap installation. As a result, volumetric measurements over time after requirement (i) being achieved were stable with no observed drift, thus guaranteeing a consistent way of determining thermal equilibrium.

2.3. Inherent thermal expansion

The coefficient of thermal expansion of water is larger than that of any component within the drainage system. This naturally results in water leaving the system (even in the absence of a soil specimen) when temperature is increased due to excess water that no longer fits in the available volume within the drainage system, even after these elements also thermally expand.

Any measurement with a soil specimen always corresponds to the combined response of the equipment and the specimen. The thermal response of the system has been believed to be predominant when compared to that of the specimen and, if not accounted for, the system's response might mask the individual response of the specimen. The equivalent volume within the drainage system that is affected by temperature is estimated to be slightly less than a third of the volume of voids of a loose specimen of Hostun sand (29 cm^3 compared to 91 cm^3). Therefore, failure to take these volumes into account will result in inaccurate assessment of the thermal expansion of the sample and emphasises the importance of performing calibrations that are reliable (i.e. stable) and repeatable.

The volume of water measured by the volume gauge that can be attributed solely to the deformation of the specimen is calculated by deducting the response of the system (obtained during calibration) from the overall measurement when a specimen is present. This is illustrated for a specimen of loose Hostun sand in Fig. 5, showing the water being drained out of the system over consecutive heating stages in which thermal equilibrium is reached. Moreover, it is important to mention that the thermal expansion of the water initially filling the specimen's voids clearly dominates the obtained response of the specimen (i.e. once the thermal expansion of the sample is isolated, the thermal expansion of the water accounts for 99.2% of the measured drained water).

3. Hydraulic conductivity tests

Due to the lack of an official guideline or standard for hydraulic conductivity tests under non-isothermal conditions, the ASTM D5084 – 16a (ASTM 2016) is used in this work as a starting point. The MKII permeameter is comparable to a flexible wall permeameter under constant head, which is achieved through the combined use of both volume gauges and respective pwp transducers.

For a rigorous use of a triaxial cell as a permeameter, it is important to be mindful of effective stress changes and ensure that testing does not affect the state of stress of the specimen. Assuming the specimen is fully saturated (B-value>0.97) and that isotropic consolidation is complete, in order to avoid changing the effective stress of the specimen, half of the pressure differential should be deducted from one end of the specimen and half of the pressure differential should be added to the other end of the specimen. For instance, considering a specimen subjected to a back pressure of 500 kPa, in order to apply a pressure differential of 6 kPa to generate upwards flow, the bottom back pressure should be set at 503 kPa and the top back pressure at 497 kPa. Following this procedure, the effective stress at mid-height of the specimen should remain constant.

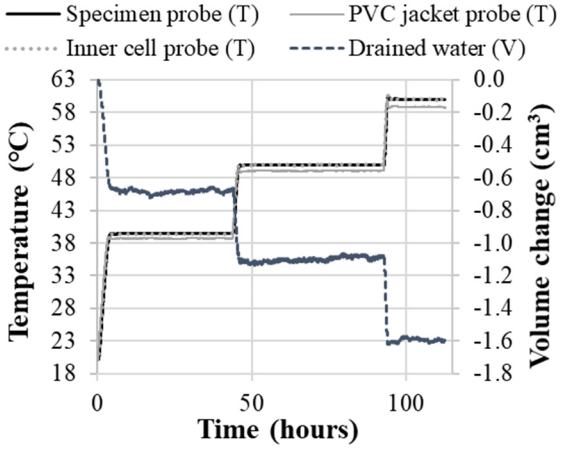

Figure 5. Consecutive heating stages on a loose Hostun sand specimen. Temperatures measured across the equipment are presented to represent the temperature field within the equipment. The corresponding volume of water that is drained out of the system, consisting of the system and specimen response, is also presented.

After setting both pressures and allowing the pressure differential to be developed along the height of the specimen, the system should reach stability. Then, for the interval in which the change of volume over time is linear and back pressures are constant, flow rate and pressure differential should be used for calculating hydraulic gradient and hydraulic conductivity. ASTM D5084 – 16a (ASTM 2016) advises that four different pressure differentials should be applied, using only values of hydraulic conductivity that differ by no more than 25% from the average of all measurements. However, since greater variations may take place for higher temperatures, six different pressure differentials were applied (ranging from 4 kPa to 9 kPa). For simplicity, pressure differential stages will be designated as "pressure steps" to avoid creating confusion with temperature stages.

3.1. Intrinsic head losses

Before discussing temperature effects on tests, it is important to discuss the intrinsic head losses of the equipment. Any confined moving fluid will experience losses in energy. In granular soils with a high permeability (and expected high seepage velocity), the energy loss in the drainage system must be considered. MKII was subjected to many modifications to reduce the system's intrinsic head losses. After the first round of improvements, a gain of 14 times in flow rate for a given pressure differential was obtained, as reported previously (Bortolotto, Taborda, and O'Sullivan 2022). After a subsequent round of improvements, which consisted of doubling the diameter of all the external tubes of the drainage lines and most of the top cap's drainage line, the gain in flow rate was over 30 to 60 times depending on the pressure differential – this corresponds to the latest and current configuration of the system.

Despite this gain in flow rate, which corresponds to a more permeable system, the ratio in flow rates between the individual response of the system and that of the expected soil is only about 1.8. This ratio is below the value of 10 required by ASTM D5084 – 16a (ASTM 2016), and, consequently, it is necessary to account for the intrinsic head losses of the equipment. As outlined in Bortolotto, Taborda, and O'Sullivan (2022), we adopted an empirical approach suggested by Head (1998) in which all parts of the drainage system were assembled as any regular test (but without a specimen) and, by applying different pressure differentials, different flow rates could be measured. Values of pressure differential were plotted against the corresponding flow rate and a regression line was then fitted to the data. This generated a calibration curve and this procedure was repeated for every target temperature. The same procedure should be done for the soil specimen, and both curves (soil and calibration) should be plotted together for each temperature. Subsequently, given a measured flow rate, the head loss attributable to the equipment can be calculated from this curve and subtracted from the measured head loss, yielding the actual head loss occurring at the soil specimen.

In summary, not all of the observed energy loss occurs within the specimen; for instance, at room temperature, the actual pressure differentials across the specimen are only 13% to 24% of the applied pressure differential. As the temperature of the system is increased and the viscosity of the water reduces, the energy lost within the system tends to reduce with temperature. For instance, at 50°C, the actual pressure differentials across the specimen correspond to 50% and 84% of the theoretical applied pressure differential of 4 kPa and 9 kPa (upwards flow), respectively.

This highlights the importance of accounting for the system's intrinsic head losses since the overall response is tremendously impacted by the system for all investigated temperatures. For the worst-case scenario (room temperature and the smallest applied pressure differential), the hydraulic conductivity could be underestimated by a factor of 7. Following the modifications mentioned above, the system's intrinsic head losses were reduced; by combining the effect of modifications and taking into account the system's head losses following the procedure outlined above, the measured hydraulic conductivity of a uniform fine sand was two orders of magnitude bigger than the original measurement using the equipment with no modification and without considering intrinsic head losses (at room temperature).

3.2. Data post-processing

After implementing the improvements outlined above (no heat reaching key instruments, intrinsic head losses taken into account, acceptable variation of instruments and measurements), attention should be turned to post-processing.

The addition of the specimen temperature probe flagged a consistent and substantial drop in temperature measured during hydraulic conductivity tests, especially after the addition of heat exchangers, since water at (or close to) room temperature is flushed through the drainage lines and has a rather limited time to warm up inside the cell, before reaching the specimen. Therefore, special attention was given to the post-processing of tests on Hostun sand and associated calibrations, with the specific objective of understanding the effect of these temperature drops on the hydraulic conductivity and intrinsic permeability.

Intrinsic permeability (K_i in m^2) is a used in this paper as a way of understanding the effect of temperature on particle arrangement and, at the same time, of excluding temperature effects on dynamic viscosity ($\mu_{w,T}$ in Pa.s) and unit weight ($\gamma_{w,T}$ in N/m^3) of water as in Eq. (1).

$$k_{h,T} = \frac{K_i \cdot \gamma_{w,T}}{\mu_{w,T}} \quad (1)$$

where $k_{h,T}$ is the hydraulic conductivity (m/s).

Drops of up to 13°C were measured by the specimen probe during upwards flow tests at 60°C. Since the applied temperature increments are either 10°C or 20°C, such drops can therefore exceed the entire increment associated with a given test stage. It is plausible that these drops might impact the interpreted hydraulic conductivity values. Therefore, results are analysed in terms of intrinsic permeability, water density, and water dynamic viscosity, which, together with the coefficient of

thermal expansion, vary considerably with temperature (Table 1).

Hydraulic conductivity tests were performed in consecutive steps of upwards flow and then downwards flow since there is finite amount of volume available in the system (~100 cm^3) as one volume gauge emptied out while the other filled up. The impact of consecutive steps was also analysed and, to complete this characterisation, tests with a waiting period were also performed. The later tests consist of performing a test in one direction, setting the original back pressure, waiting until the specimen temperature (as measured by the specimen probe) goes back to its initial value and only then proceeding with the test in the opposite flow direction.

Table 1. Water dynamic viscosity and unit weight as a function of temperature

	Temperature (°C)				
	20	**30**	**40**	**50**	**60**
Dynamic viscosity (Pa·s)	1.002	0.879	0.653	0.522	0.466
Unit weight (kN/m^3)	9.792	9.767	9.733	9.688	9.634

Tests with a waiting period gave the highest observed drop in temperature since the water just flushed out of the warm specimen had time to cool down before being pushed back through the specimen. Therefore, this approach was judged worse than the regular approach of performing consecutive steps of upwards and downwards flow straight way.

For both scenarios, with and without the waiting period, temperatures right at the beginning and end of each pressure step, as well as the respective average of these extreme values and the target temperature (of each stage) were used when calculating the intrinsic permeability of the specimen (Table 2). Since hydraulic conductivity is reported more often than intrinsic permeability, hydraulic conductivity was then back-calculated only for the purpose of understanding the impact of the drops in temperature.

Table 2. Loose Hostun sand hydraulic conductivity ("HC") and intrinsic permeability ("IP") at the third stage of heating (40°C) obtained with ("Wait.") and without ("Dir.") waiting period between consecutive pressure steps.

		Analysed temperature			
		Beg.	**End**	**Aver.**	**Target**
HC (m/s)	**Dir.**	2.36E-04	2.50E-04	2.42E-04	2.32E-04
	Wait.	2.65E-04	3.09E-04	2.96E-04	2.63E-04
IP (m^2)	**Dir.**	1.58E-11	1.67E-11	1.62E-11	1.55E-11
	Wait.	1.77E-11	2.07E-11	1.98E-11	1.76E-11

For the studied temperature range, the water density varied by only 1.5% (Table 1), whereas water dynamic viscosity changed by more than 50%. The observed drop in 13°C, while performing tests at 50°C, gave a 36% change in the intrinsic permeability. A maximum variation of 32% amongst the entire population of (back-calculated) hydraulic conductivities was observed in tests on loose Hostun sand at 40°C (Table 2). This corresponds to an amplitude of $1.60 \cdot 10^{-4}$ m/s. ASTM D5084 – 16a (ASTM 2016) accepts a variation of ±25% while determining hydraulic conductivity for materials with permeability higher than $1 \cdot 10^{-10}$ m/s. In terms of intrinsic permeability, the maximum observed relative variation was about 16% – while disregarding tests with "waiting" period.

As outlined above, water that is slightly colder than the specimen is pushed into the soil specimen. This means that the target temperature is the highest temperature out of the four analysed (e.g. Table 2), giving the smallest dynamic viscosity, thus leading to the lowest value of intrinsic permeability out of the four calculated from each analysed temperature. The target temperature has consistently been the lower value (out of the four analysed) for tests performed at 30°C or higher temperatures, emphasising the importance of dynamic viscosity.

Although the specimen temperature probe provides valuable information about the temperature of the specimen, measurements only reflect the actual state of the specimen while there is no forced flow of water. When water at a temperature other than the target temperature is flushed into the specimen, heat exchange occurs. As colder water is pushed into the specimen, it is expected that heat will move from the specimen to the water. Furthermore, because the most important heat transfer mechanism in the specimen (and being registered by the probe) is convection, it is believed that measurements from this probe do not reflect the actual specimen's temperature.

While determining the actual specimen temperature during hydraulic conductivity tests is not possible, tests with a waiting period provided insightful information on this matter. A maximum volumetric variation (after each pressure step) of 0.23 cm^3 was observed during the waiting period. This small variation corresponds to about 0.25% of the volume of voids in the loose Hostun sand specimen and may indicate that the specimen and the soil skeleton are unaffected by heat exchange and, therefore, its thermo-hydromechanical state should be unchanged.

4. Concluding remarks

This study has highlighted the intrinsic limitations of non-isothermal hydraulic conductivity tests on granular soils. Requirements for the testing equipment, including details of changes introduced to the Imperial College MKII Permeameter to improve its accuracy, were also discussed.

Thermal cameras were used to identify hot spots along the external surface of the equipment and instruments. The transient nature of heat transfer through the various components of the equipment was observed

by monitoring the surface of key elements, so that any attempt to calibrate at different temperatures were considered unlikely to be successful. After identifying the hot spots, it was possible to introduce two main modifications that lowered the superficial temperature of both volume gauges and pwp transducers to virtually room temperature, which implied that calibrations at room temperature can be employed with confidence. Coiled-shaped copper tubes effectively worked as heat exchangers by reducing the temperature at the entrance of volume gauges by more than 15°C when testing at 60°C. Spacers that physically separate the pwp transducers from the flow of warm water (leaving the specimen) reduced the temperature on the surface of the pwp transducers by approximately 8°C and their effectiveness still requires further investigation.

The specimen temperature probe was essential to establish the temperature field within the specimen and equipment and to determine the time required for the system to reach thermal equilibrium. Moreover, while performing calibrations with a PVC dummy sample, this probe provided crucial information to determine the origin of abnormal drifts in the volume gauges, which strongly suggested non-recoverable deformations were taking place at the drainage lines. This then led to switching the drainage lines' material to stiffer options.

The system's total thermal expansion proved to be important; the volume of water affected (by temperature) reached one third of the volume of voids of a loose sandy specimen. This can lead to incorrect evaluation of thermally-induced volumetric strains.

Given the high variation dynamic viscosity of water (>50%) at different temperatures within the studied range (20 to 60°C), the observed temperature drop (up to 13°C) flagged by the specimen temperature probe meant that the specific temperature value used when post-processing the results of the tests must be selected carefully. Consequently, although it might be more interesting to use average temperature values for each pressure step, using the target temperature of different stages seems to result in (back-calculated) hydraulic conductivity within the expected range. This also corresponds to the smallest value of intrinsic permeability since the target temperature also tends to be higher than all other studied temperatures, and hence lead to the use of the smallest value of dynamic viscosity.

In summary, this paper analysed relevant protocols to perform and interpret data related to hydraulic conductivity tests conducted at different temperatures. Thermal performance and thermal effects on the instruments used in the Imperial College MKII permeameter were discussed. However, despite the success of the modifications described in this paper, their extrapolation to other equipment and, indeed, materials, should be undertaken with care.

Acknowledgements

This project is funded through Marie SKŁODOWSKA-CURIE Innovative Training Network MATHEGRAM, the People Programme (Marie SKŁODOWSKA-CURIE Actions) of the European Union's Horizon 2020 Programme H2020 under REA grant agreement No. 813202.

References

Abdelaziz, S. L., and S. Morteza Zeinali. "Calibrating Thermomechanical Triaxial Cells for Transient Thermal Loads", Geotech Test J, 45(1), pp. 201-211, 2022. https://doi.org/10.1520/GTJ20200299

ASTM "D5084-16a: Standard test methods for measurement of hydraulic conductivity of saturated porous materials using a flexible wall permeameter", ASTM International, USA, 2016.

Azeiteiro, R. J. N., Coelho, P. A. L. F., Taborda, D. M. G., and Grazina, J. C. D. "Critical State–Based Interpretation of the Monotonic Behavior of Hostun Sand", J Geotech Geoenviron Eng, 143(5), 2017. https://doi.org/10.1061/(ASCE)GT.1943-5606.0001659

Bortolotto, M. S., D. M. G. Taborda, and C. O'Sullivan. "Thermal effects on the hydraulic conductivity of a granular geomaterial", In: 20th ICSMGE 2022: A geotechnical discovery down under, Sydney, Australia, 2022, pp. 5017-5022.

Campanella, R. G., and J. K. Mitchell. "Influence of temperature variations on soil behaviour", ASCE J Soil Mech Found Div, 4(3), pp. 709-734, 1968.

Cekerevac, C., L. Laloui, and L. Vulliet. "A Novel Triaxial Apparatus for Thermo-Mechanical Testing of Soils", Geotech Test J, 28(2), pp. 161-170, 2005. https://doi.org/10.1520/GTJ12311

Chen, S. X. "Thermal conductivity of sands", Heat Mass Transfer, 44, pp. 1241–1246, 2008. https://doi.org/10.1007/s00231-007-0357-1

Chen, S., L. Zdravkovic, and J. A. H. Carraro. "Thermally induced pore water pressure of reconstituted London clay", In: E3S Web Conf. 92, 10003, Glasgow, UK, 2019. https://doi.org/10.1051/e3sconf/20199210003

Russell Coccia, C., and J. McCartney. "A Thermo-Hydro-Mechanical True Triaxial Cell for Evaluation of the Impact of Anisotropy on Thermally Induced Volume Changes in Soils", Geotech Test J, 35(2), pp. 227-237, 2012. https://doi.org/10.1520/GTJ103803

Finn, F. "The effect of temperature on the consolidation characteristics of remolded clay", In: Symposium on Consolidation Testing of Soils, New Jersey, USA, 1952, pp. 65-71.

Head, K. H. 1998. Manual of soil laboratory testing. Volume 3: Effective stress tests, 2nd ed. John Wiley & Sons Ltd., England.

Jaradat, K. A., and S. L. Abdelaziz. "Thermomechanical Triaxial Cell for Rate-Controlled Heating-Cooling Cycles", Geotech Test J, 43(4), p. 1022-1036, 2020. https://doi.org/10.1520/GTJ20180354

Kirkham, A. D., A. Tsiampousi, and D. M. Potts. "Temperature-controlled oedometer testing on compacted bentonite",In: 7th International Conference on Unsaturated Soils, Hong Kong, China, 2018.

Liu, H., H. Liu, Y. Xiao, J. S. McCartney. "Influence of Temperature on the Volume Change Behavior of Saturated Sand", Geotech Test J, 41(4), pp. 747-758, 2018. https://doi.org/10.1520/GTJ20160308

Martinez-Calonge, D. "Thermo-mechanical behaviour and thermal properties of London clay", PhD Thesis, Imperial College London, 2017. https://doi.org/10.25560/69756

Mitchell, J. K., and K. Soga. "Fundamentals of Soil Behavior", 3rd ed., John Wiley & Sons Inc., New Jersey, USA, 2005.

Pan, Y., J. B. Coulibaly, and A. F. Rotta Loria. "An experimental investigation challenging the thermal collapse of sand", Géotechnique, 2022. https://doi.org/10.1680/jgeot.21.00309